ELSEVIER

Coordination Chemistry Reviews
190–192 (1999) 331–355

COORDINATION CHEMISTRY REVIEWS

www.elsevier.com/locate/ccr

Structural properties of the nickel ions in urease: novel insights into the catalytic and inhibition mechanisms

Stefano Ciurli [a,*], Stefano Benini [b], Wojciech R. Rypniewski [b], Keith S. Wilson [c], Silvia Miletti [a], Stefano Mangani [d]

[a] *Institute of Agricultural Chemistry, University of Bologna, Viale Berti Pichat 10, I-40127 Bologna, Italy*

[b] *European Molecular Biology Laboratory, c/o DESY, Notkestraße 85, D-22603 Hamburg, Germany*

[c] *Department of Chemistry, University of York, Heslington, York YO1 5DD, UK*

[d] *Department of Chemistry, University of Siena, Pian dei Mantellini 44, I-53100 Siena, Italy*

Accepted 13 March 1999

Contents

Abstract

This work provides a comprehensive critical summary of urease spectroscopy, crystallography, inhibitor binding, and site-directed mutagenesis, with special emphasis given to the

Abbreviations: JBU, jack bean urease; KAU, *Klebsiella aerogenes* urease; BPU, *Bacillus pasteurii* urease; β-ME, β-mercaptoethanol; PPD, phenylphosphorodiamidate; AHA, acetohydroxamic acid; XAS, X-ray absorption spectroscopy; EXAFS, extended X-ray absorption fine structure; CD, circular dichroism; MCD, magnetic circular dichroism.

* Corresponding author. Tel.: +39-051-259794; fax: +39-051-243362.
E-mail address: sciurli@agrsci.unibo.it (S. Ciurli)

PII: S0010-8545(99)00093-4

relationships between the structural features of the Ni-containing active site and the physico–chemical and biochemical properties of this metallo-enzyme. In addition, the recently determined structure of a complex between urease and a transition state analogue is discussed as it leads to a novel, thought-provoking proposal for the enzyme mechanism.

Keywords: Urease spectroscopy; Site-directed mutagenesis; Inhibitor binding

1. Biological background

Urea is formed in large quantities as a product of catabolism of nitrogen-containing compounds, each human producing, for example, ca. 10 kg of urea per year [1]. Urea spontaneously decomposes with a half-life of ca. 3.6 years [2], and without an efficient degradation process, it would rapidly accumulate causing severe environmental problems. The biological catalyst for the hydrolytic decomposition of urea is the enzyme urease (urea aminohydrolase E.C. 3.5.1.5). Urease may be thought to represent the paradigm in the development of biological inorganic chemistry. The first enzyme to be crystallized, from the plant source *Canavalia ensiformis* (jack bean) [3], was also the first protein shown to contain nickel in the active site [4]. This discovery stimulated efforts to unravel the chemistry of such a rare microelement in other biological settings, leading to the discovery of the presence of nickel in CO–dehydrogenase from photosynthetic bacteria [5], methyl coenzyme M reductase-bound factor Ni-F430 from methanogenic bacteria [6,7], bacterial Ni,Fe–hydrogenase from several microorganisms [8], acetyl–CoA synthase from methanogenic and acetogenic bacteria [9], and superoxide dismutase from actinomycetes [10,11].

Urease catalyzes the hydrolysis of urea in plants, algae, fungi, and several microorganisms [12,13], in the final step of organic nitrogen mineralization to produce ammonia and carbamate. This process occurs 10^{14} times faster than the uncatalyzed reaction [14], with a half-time in the order of microseconds. The carbamate produced during this reaction spontaneously decomposes, at physiological pH, to give a second molecule of ammonia and bicarbonate [13–16].

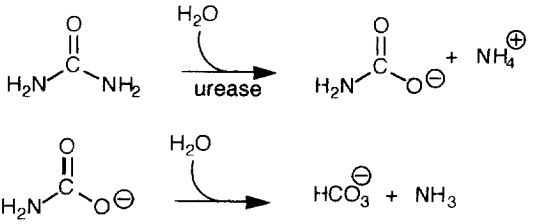

The hydrolysis of the reaction products causes an abrupt overall pH increase, the major cause for the negative side effects of the action of urease both for human and

animal health, and for agriculture. Urease serves as a virulence factor in human and animal infections of the urinary and gastrointestinal tracts, being involved in kidney stone formation, catheter encrustation, pyelonephritis, ammonia encephalopathy, hepatic coma, and urinary tract infections [13,16,17]. The ureolytic activity of *Helicobacter pylorii* is also the major cause of pathologies (including cancer) induced by gastroduodenal infections by such microorganisms. In another context, urea is largely used worldwide as a soil fertilizer, representing a fundamental source of nitrogen for plant nutrition [18]. This is made possible by the large amount of urease in soil, present both in living ureolytic bacteria [19] and as extracellular urease. The latter is found aggregated with clays and humic substances, which prevent its degradation by extracellular proteolytic enzymes and microorganisms [20–22]. The efficiency of soil nitrogen fertilization with urea is severely decreased by this widespread urease activity, which causes the release of large amounts of ammonia in the atmosphere and further induces plant damage by ammonia toxicity and soil pH increase, thereby posing significant environmental and economic problems [21].

In conclusion, the health and environmental impact of urease activity is enormous, and control of the rate of urea hydrolysis by using urease inhibitors would lead to enhanced efficiency of urea nitrogen uptake by plants and to improved therapeutic strategies for treatment of infections by ureolytic bacteria. Several classes of molecules (di-phenols, quinones, hydroxamic acids, phosphoramides and thiols) have been tested as urease inhibitors in medicine [13,16,23]. Urease inhibitors have also been proposed to control urea hydrolysis in soil [13,24–31]. In particular, phosphoramides have received considerable attention as urease inhibitors [27,30], the best example being N-(*n*-butyl)thiophosphoric triamide (NBPT) [32–37]. However, the efficiency of the presently available inhibitors is low, and negative side effects on humans [13,16,38,39] and on the environment [13,40] have been reported. The discovery of urease inhibitors has so far relied upon extended screen tests [41]. A structure-based molecular design approach for the discovery of new and efficient urease inhibitors relies upon the elucidation of the structure of the active site of this enzyme and of its mechanism. The highly conserved amino acid sequences of all known ureases [16,42] and the constant presence of two Ni ions and of their ligands in the active sites [14] infer a common catalytic pathway. Therefore, the determination of the structure of ureases isolated from different sources will establish the essential common features of these enzymes. These analogies will provide a better understanding of the chemistry of the catalysis, and also allow rational design of inhibitors capable of functioning with a broad range of microbial ureases.

2. Spectroscopic investigations of the urease active site structure

The presence of six-coordinate octahedral Ni(II) in jack bean urease (JBU) was first proposed on the basis of optical absorption spectroscopic studies [4,43,44], which almost completely ruled out the presence of four- or five-coordinated nickel

ions. Early EXAFS studies on JBU confirmed these results, and indicated the presence of pseudooctahedral Ni ions coordinated to three N atoms at 2.04 Å, two O atoms at 2.07 Å, and one O atom at 2.25 Å [45,46]. The presence of Ni-bound His residues was also suggested [45]. Later, new X-ray absorption spectroscopy data were interpreted with a model involving distorted octahedral Ni(II) ions bound to five or six (N,O) donors at an average distance of 2.06 Å [47]. Magnetic susceptibility experiments indicated that, in JBU, high spin octahedrally coordinated Ni(II) ($S = 1$) ions are weakly antiferromagnetically coupled ($J = -6.3$ cm^{-1}) [48]. This conclusion was subsequently disputed [49], but the diamagnetism resulting from binding of the competitive inhibitor β-mercaptoethanol (β-ME) [48], and the evidence that this binding involved a ligand exchange in the coordination sphere of nickel [47], suggested the presence, in the active site of JBU, of two closely spaced Ni(II) ions which, in the presence of β-ME, are strongly antiferromagnetically coupled through a bridging thiolate. This conclusion received further support from later EXAFS (extended X-ray absorption fine structure) studies, which indicated the appearance of a new peak in the Fourier transform upon addition of β-ME to JBU. This peak could be fitted using a model involving the presence of two Ni ions 3.26 Å apart [50]. This study also indicated the presence of His residues bound to pentacoordinated Ni(II) ions, with a coordination environment of the type $Ni(His)_x(N,O)_{5-x}$, with $x = 2$ or 3 [50].

Ni-edge X-ray absorption spectroscopy (XAS) studies carried out on urease from *Klebsiella aerogenes* (KAU) and *Bacillus pasteurii* (BPU), also containing a binuclear nickel active site [51,52], give a picture of the active site which is extremely similar to that of JBU [50,53]. This resemblance is to be expected considering the homology in amino acid sequence between subunits α, β, and γ of the heteropolymeric KAU [54] and BPU [55] with the 271–840, 132–237, and 1–101 portions, respectively, of the homopolymeric JBU (subunit M_r 90 770) [56]. Hereafter, the amino acid numbering used in the discussion will follow that of each different enzyme except when stated explicitly, and the high homology among the different ureases will be evident. In the case of BPU, the XAS edge and EXAFS analysis of the phenylphosphorodiamidate (PPD)-inhibited enzyme indicate that the first coordination sphere is not significantly affected by the inhibitor binding, and that phosphorous is present in the outer shells [53], a result interpreted as directly showing, for the first time, the binding of this inhibitor to the Ni center. All XAS studies on ureases provided a very self-consistent picture for the average Ni environment in urease, which contrasted sharply with that resulting from the first crystal structure of the enzyme that appeared in the literature.

3. Crystallographic studies of the native enzyme

The report of the X-ray crystal structure of KAU provided a detailed 3-D structural model of the active site [57]. In native KAU (Fig. 1), two well-ordered Ni atoms (B-factor = 19 and 15 $Å^2$) are held at a distance of 3.6 Å by the bridging carboxylate group of the carbamylated $Lys^{\alpha 217}$ residue: Ni(1) appears to be bound

to His$^{\alpha 246}$ Nδ and to His$^{\alpha 272}$ Nε, while Ni(2) is bound to His$^{\alpha 134}$ Nε, to His$^{\alpha 136}$ Nε, and to Asp$^{\alpha 360}$ Oδ1. In the first model proposed (PDB code 1KAU, Table 1) [57], Ni(1) appears to be tri-coordinated, while Ni(2) is penta-coordinated in a distorted trigonal bipyramidal geometry (or distorted square pyramidal, with His$^{\alpha 136}$ Nε as the apical ligand). The fifth ligand to Ni(2) is a well-ordered water molecule (W1, B-factor = 14 Å^2) proposed to act as the catalytic nucleophile [57]. An additional water molecule (W170, B-factor = 25 Å^2) was found in the active site cavity, hydrogen bonded to Wat-1, and potentially interacting with Ala$^{\alpha 363}$ O, Gly$^{\alpha 277}$ O, and His$^{\alpha 320}$ Nε through hydrogen bonds (Fig. 1). The structure shows a hydrogen bond between His$^{\alpha 320}$ Nδ and the carboxylic group of Asp$^{\alpha 221}$: the authors suggested in this report that His$^{\alpha 320}$ Nε is deprotonated and acts as the general base [57]. Later, the same authors instead proposed that His$^{\alpha 320}$ Nε is protonated at pH 7.5 and could act as the general acid [58,59] even though it was known that its pK_a is 6.5 [60,61]. In native KAU, His$^{\alpha 219}$, known to be involved in substrate binding [61], is placed at 3.1 Å from Ni(1), pointing toward the active site cavity with its protonated Nε atom: this feature suggested that it could act as hydrogen bonding donor to the oxygen of urea, thereby helping position and polarize the substrate [42]. However, in this structure no hydrogen bonding partner was found, as His$^{\alpha 219}$ pointed to an empty coordination site of Ni(1) (Fig. 1). The model deposited with the PDB code 1KAU was derived from merging data obtained with two different crystals [57]. In the same report, another model was only briefly mentioned, derived

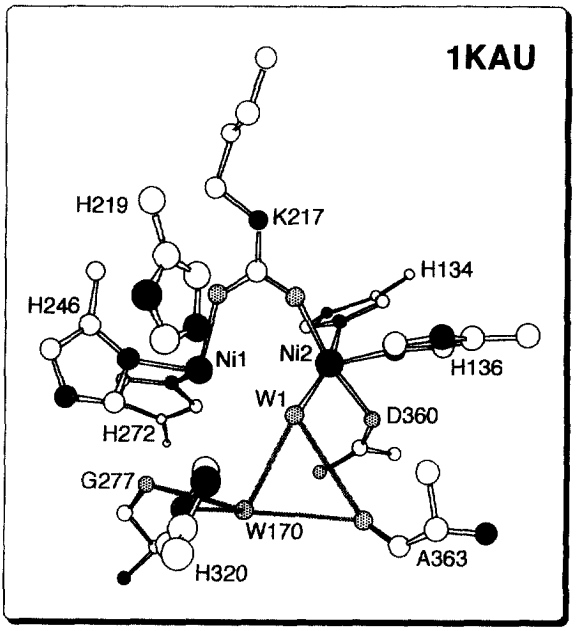

Fig. 1. Model of the active site of native KAU, showing the position of selected relevant residues. In this figure, and in all the following figures, Ni atoms are shown in black, C atoms in white, N atoms in dark grey and O atoms in light grey. H-bonds are shown as solid lines. All residues are sized according to their different depths. The PDB code is indicated.

Table 1
Selected crystallographic parameters for urease structures

PDB code	Resolution (Å)	Data completeness (%)	Redundancy	R-factor (%)
1KAU	2.2	92	7.8	18.2
2UBP	2.00	96.7	13.1	16.2
1FWJ	2.2	not reported	not reported	17.3
1KRA	2.3	98	7.3	19.0
1KRB	2.5	98	3.1	17.9
1KRC	2.5	99	3.3	18.0
1FWI	2.0	not reported	not reported	17.0
1FWA	2.0	94	3.3	16.9
1FWB	2.0	97	3.4	16.9
1FWC	2.0	96	3.3	16.8
1FWD	2.0	96	2.8	16.9
1FWF	2.0	97	3.5	17.1
1FWG	2.0	92	2.3	17.6
1FWH	2.0	91	2.3	17.9
1A5K	2.2	92	5.1	17.8
1A5L	2.2	93	2.0	18.6
1A5M	2.0	90	1.8	19.4
1A5N	2.4	100	4.0	16.7
1A5O	2.5	100	4.1	18.1
1UBP	1.65	98.7	10.2	16.0
1FEW	2.0	96	2.3	20.4
3UBP	2.00	99.9	13.4	15.8

from merging data obtained using three additional crystals, which differed from the one described above in displaying uninterpreted electron density between the two Ni ions, with appropriate dimension to accommodate a urea molecule or a carbonate ion [57].

The model proposed for native KAU, involving a tri-coordinated and a penta-coordinated Ni ions, was in conflict with all previous spectroscopic data on KAU [50] and JBU [44–48,50,62] as well as with XAS data on BPU [53] which indicated the presence of hexa- or penta-coordinated slightly distorted octahedral Ni ions. It has been remarked that the inconsistencies between the spectroscopic and structural analyses were probably due to the absence, in the crystallographic model, of light, non-protein ligands, possibly water molecules or hydroxide ions, bound to the Ni ions [53]. These were not detected in the first model of KAU because of the relatively low resolution and lack of completeness of the diffraction data set [57]. The understanding of the catalytic mechanism of urea hydrolysis, for which the role of water molecules (or hydroxide ions) in the active site is crucial [2], requires the determination of the positions of water molecules in the active site of urease, a topic which has been the subject of intense discussion [59,63]. Data with higher resolution and completeness were therefore necessary to resolve the discrepancies between the coordination geometry of Ni(II) found in urease and the stereoelectronic behavior of this metal ion in synthetic coordination compounds, for which no cases of coordination geometries analogous to that proposed for KAU are known.

In order to solve the 'water problem' in the active site of urease, the enzyme from BPU was purified [52], crystallized [64], and synchrotron X-ray cryogenic data were collected on a single crystal [64]. The description of the structural model for native BPU (PDB code 2UBP, Table 1) has been reported [65].

In BPU, the electron density in the active site is very well defined, providing a clear picture of the Ni coordination. The two metal ions are bridged by the carboxylate group of the carbamylated $Lys^{\alpha 220*}$, bound to Ni(1) through Oθ1 and to Ni(2) through Oθ2. Ni(1) is further coordinated by $His^{\alpha 249}$ Nδ and $His^{\alpha 275}$ Nε, while Ni(2) is bound to $His^{\alpha 137}$ Nε, $His^{\alpha 139}$ Nε, and $Asp^{\alpha 363}$ Oδ1 (Fig. 2). Both Ni ions are well ordered (B-factors of 19 and 18 $Å^2$ for Ni(1) and Ni(2), respectively) and separated by 3.7 Å. In the above features, the BPU active site is essentially identical to that of KAU. However, for BPU the difference Fourier maps unambiguously show a tetrahedrally shaped electron density in the vicinity of the two Ni ions, symmetrically positioned between the metal centers, suggesting the presence of non-protein ligands completing the metal coordination spheres [65]. Four water/hydroxide molecules, three of which directly bound to the metal ions, where modelled with full occupancy, resulting in B-factors which indicate a high degree of order (17–23 $Å^2$). One of these (WB) symmetrically bridges the two Ni ions, whereas the other two (W1 and W2) complete the coordination polyhedron around the Ni ions. Ni(1) has a penta-coordinate distorted square–pyramidal geometry, with a basal plane consisting of $His^{\alpha 275}$ Nε, $His^{\alpha 249}$ Nδ, W1 and WB, the apical ligand being $Lys^{\alpha 220*}$ Oθ1, whereas Ni(2) has a hexa-coordinate distorted octahedral geometry

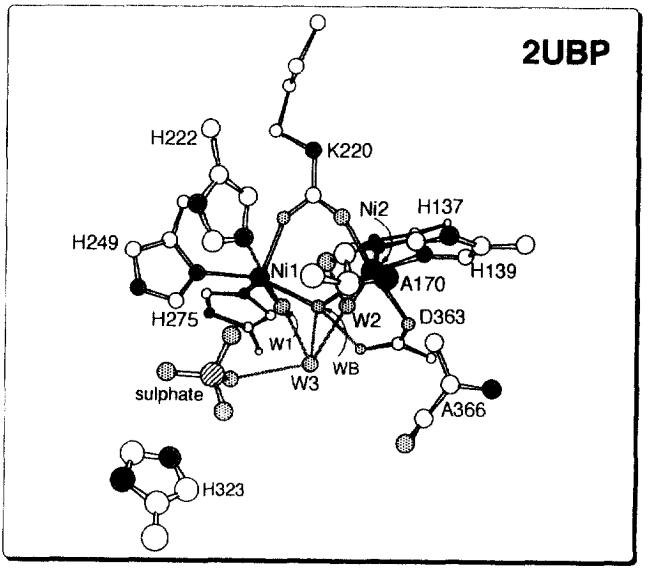

Fig. 2. Model of the active site of native BPU, showing the position of selected relevant residues. Atoms and bonds as in Fig. 1. All residues are sized according to their different depths. The PDB code is indicated.

(Fig. 2). A fourth water molecule, W3, strongly interacts with WB (at 2.3 Å), W1 (at 2.2 Å), and W2 (at 2.4 Å), through hydrogen bonds. The angles formed by Ni(1,2)–W(1,2,B)–W(3) are very close to tetrahedral. W3 is at the center of additional possible multiple hydrogen bonding interactions, being 3.3 Å from $Asp^{\alpha 363}$ Oδ2, 3.4 Å from $Gly^{\alpha 280}$ O, and 2.7 Å from another water molecule situated towards the opening of the active site cleft. W3 is at hydrogen bonding distance (3.0 Å) from the oxygen atom of a sulfate ion found in the cavity (Fig. 2). The sulfate ion is located between the four water/hydroxide cluster and the nearby $Arg^{\alpha 339}$, in a position occupied, in native KAU, by the imidazole ring of $His^{\alpha 323}$ ($His^{\alpha 320}$ in native KAU). $Arg^{\alpha 339}$ extends from the very bottom of the active site cleft, and forms a strong salt bridge with the sulfate ion, which in turn forms a hydrogen bond with $His^{\alpha 323}$ Nε (at 2.7 Å). The presence of sulfate is probably due to its high concentration in the crystallization buffer. The crystals of KAU were also obtained from sulfate-rich solutions, but sulfate binding is not described in any of the published structures [57–59,63,66,67].

The assignment of the protonation state of W1 and W2 as water molecules at the optimum pH for BPU activity (pH 8.0 [68]) is suggested by the value of the first dissociation constant for $Ni(H_2O)_6^{2+}$ (pK_a 10.6) [69]. In water-bridged bimetallic complexes, the first pK_a for the bridging water decreases significantly to very acidic values, while the pK_a for hydroxide deprotonation is slightly lower than the pK_a of the first ionization of a water bound to a single Ni ion [69]. Therefore, the estimated pK_a for the deprotonation of the Ni bridging hydroxide (ca. 9–10) suggests that, at pH 8.0, WB is in the hydroxo form. In this context, WB is at hydrogen bonding distance from $Asp^{\alpha 363}$ Oδ2 (2.5 Å) (Fig. 2).

Overall, in native BPU two different types of ligands bridge the binuclear Ni cluster (the carboxylate group of the carbamylated lysine and the hydroxide molecule), accounting for the observation of weak antiferromagnetic coupling [48]. The increase of the antiferromagnetic coupling constant observed above pH 9 [49] can be explained by the deprotonation of the bridging hydroxide to the oxide form, which mediates a more efficient magnetic interaction than hydroxide.

Meanwhile, a more recent model for native KAU was reported (PDB code 1FWJ, Table 1), which showed a topology for the solvent molecules in the active site equivalent to that found in native BPU [63,67]: however, the protonation state of these water molecules was not discussed, no electron density for the wild-type enzyme has ever been shown, and the simultaneous presence of these solvent molecules was ruled out because the distance among the three Ni-bound water molecules (2.0–2.5 Å) was considered too short [59,63]. The distances between WB, W1, and W2 in native BPU are also short (2.1–2.2 Å) compared to the usual interatomic distance in a regular octahedral $[Ni(H_2O)_6]^{2+}$ ion (ca. 2.9 Å) [70]. However, for native BPU this has not been explained as due to partial occupancy as in the case of KAU, but rather as a consequence of the peculiarities of the active site cavity [65]. The presence of a four-centered hydrogen bonding network involving a proton located in the center of the tetrahedron constituted by W(1), W(2), W(3) and W(B) explains the structural features of the four water/hydroxide cluster [65]. Furthermore, a detailed analysis of the interactions between W1 or W2 and

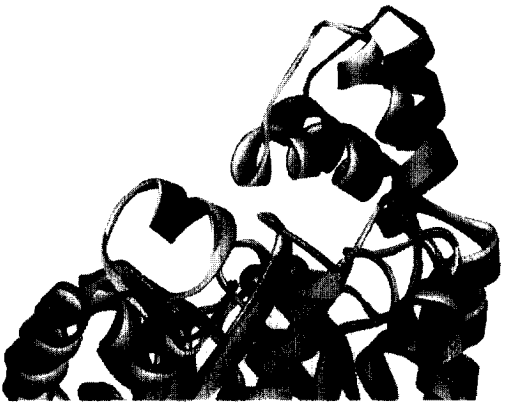

Fig. 3. Different conformations adopted by the helix-turn-helix motif of the flexible flap in native BPU (dark) and KAU (light). The two Ni ions of the native enzyme are shown as spheres of arbitrary radius.

the nearby amino acids reveals the presence of close van der Waals contacts between W1 and $His^{\alpha 249}$ Cε (3.5 Å), $His^{\alpha 249}$ Nδ (3.2 Å), $Gly^{\alpha 280}$ O (3.7 Å), and $Lys^{\alpha 220*}$ Oθ1 (3.4 Å), and between W2 and $His^{\alpha 139}$ Cε (3.2 Å), $His^{\alpha 139}$ Nε (3.0 Å), $Ala^{\alpha 366}$ Cβ (3.3 Å) and $Lys^{\alpha 220*}$ Oθ2 (3.0 Å). Moreover, W1 is at 2.9 Å from $His^{\alpha 222}$ Nε, which is protonated and acts as a hydrogen bonding donor (Fig. 2), as deduced from the interaction of $His^{\alpha 222}$ Nδ with the peptide NH group of $Asp^{\alpha 224}$ (at 2.9 Å). In contrast, W2 forms a strong hydrogen bond with $Ala^{\alpha 170}$ O (at 2.9 Å), which acts as hydrogen bonding acceptor (Fig. 2).

The overall architecture of native BPU is essentially identical to that of native KAU, the most evident conformational difference occurring in the helix-turn-helix motif lining the active site cleft in the α subunit [65]. This motif is characterized, in KAU, by high mobility as judged by the temperature factors [63], and this mobility has been proposed to be important for regulating both the access of the substrate to the active site and the release of the reaction products [57,66]. This flap also shows large atomic displacement parameters in native BPU [65], but is in a different conformation compared to native KAU [57]. In particular, the flap can be considered 'open' in BPU as opposed to being 'closed' in KAU, directly revealing the existence of two possible distinct conformations (Fig. 3).

The observation of this conformational difference allows the analysis of the effects induced on the position of the amino acid side chains lining the active site cavity. In both native BPU and KAU structures, the positions of conserved amino acid residues not involved in Ni binding but thought to be important in the catalytic mechanism ($Ala^{\alpha 170}$, $His^{\alpha 222}$, $Gly^{\alpha 280}$, $Cys^{\alpha 322}$, $His^{\alpha 323}$, $His^{\alpha 324}$, $Arg^{\alpha 339}$, and $Ala^{\alpha 366}$) (BPU consensus sequence) are largely invariant, except for $Cys^{\alpha 322}$, $His^{\alpha 323}$, and $His^{\alpha 324}$. In particular, in native BPU ('open' conformation) $His^{\alpha 323}$ is displaced by ca. 5 Å away from W3 with respect to the position of the homologous residue $His^{\alpha 320}$ in native KAU ('closed' conformation, cf. Figs. 1 and 2). In KAU, $His^{\alpha 320}$ is located at hydrogen bonding distance to W170 (corresponding to W3 in BPU),

whereas in BPU the corresponding interaction between $His^{\alpha 323}$ and W3 is hindered by the presence of the sulfate ion. The opening of the flap in native BPU induces also a large shift of the position of $Cys^{\alpha 322}$ (ca. 4 Å) and of $His^{\alpha 324}$ (ca. 7 Å) with respect to the position of the homologous residues $Cys^{\alpha 319}$ and $His^{\alpha 321}$ in native KAU, when the flap is closed. Furthermore, in the latter case the carbonyl oxygen of $Ala^{\alpha 363}$ is at hydrogen bonding distance from W1 (corresponding to W2 in BPU), whereas, when the flap is open as in BPU, the corresponding residue $Ala^{\alpha 366}$ is rotated away, at a distance (5.1 Å from W2) that does not allow formation of hydrogen bonds. The position of the side chain of $Arg^{\alpha 339}$, stretching from the very bottom of the cleft toward the active site Ni ions, is not influenced as much as for $Cys^{\alpha 322}$, $His^{\alpha 323}$, and $His^{\alpha 324}$ by the flap opening, which induces a shift of the terminal guanidinium group of only ca. 1 Å away from the Ni ions with respect to the position of the homologous $Arg^{\alpha 336}$ in KAU.

The structure of apo-urease from *K. aerogenes*, in which the Ni ions were chemically removed simply by lowering the pH in the presence of chelating agents, reveals that such treatment causes the de-carbamylation of the bridging lysine residue (PDB code 1KRA, Table 1) [42]. The model shows the absence of both Ni(1) and Ni(2), and the presence of a well ordered water molecule (W173, B-factor = 19 $Å^2$) in the place of Ni(2), hydrogen bonded to $His^{\alpha 134}$ Nε, $His^{\alpha 136}$ Nε, and $Asp^{\alpha 360}$ Oδ1 (Fig. 4). All other α-carbon atoms show a very small rms deviation (0.2 Å) with respect to the holo-enzyme, indicating an overall rigidity of the protein, and in particular of the active site. This indicates that the architecture of urease is designed to bind the Ni ions in a well-defined mode without having to undergo conformational rearrangements that might destabilize the functioning enzyme and increase the Ni dissociation equilibrium constant.

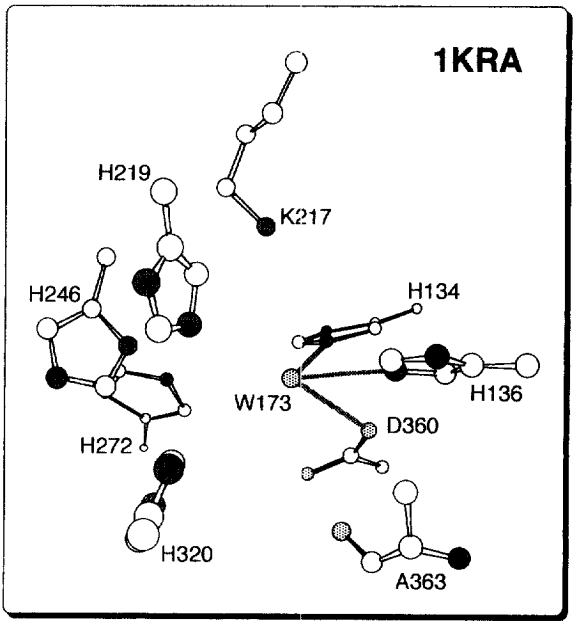

Fig. 4. Model of the active site of apo-KAU, showing the position of selected relevant residues. Atoms and bonds as in Fig. 1. All residues are sized according to their different depths. The PDB code is indicated.

4. Crystallographic studies of urease mutants

Several mutants of KAU have been structurally investigated in order to rationalize their enzymatic behavior. The His$^{\alpha 219}$Ala mutant, for example, features a much lower affinity for the substrate urea (K_m = 1100 mM as compared to K_m = 2.3 mM for the wild-type) and a ca. 30-fold decrease of K_{cat} [61], indicating a direct or indirect role for His$^{\alpha 219}$ in substrate binding. The structure of this mutant (PDB code 1KRB, Table 1) shows substantial identity with native KAU (rms deviation of the Cα chain of 0.2 Å), including the position of the two water molecules in the vicinity of the Ni ions, except with the obvious absence of His$^{\alpha 219}$ (Fig. 5).

The His$^{\alpha 320}$Ala mutant, in contrast, displays only a small change in K_m, but a ca. 30 000-fold decrease in K_{cat} with respect to the wild-type enzyme [61], while it does not show the His$^{\alpha 320}$ dependent pK_a 6.5 observed for wild-type urease [60,61]. The structure of His$^{\alpha 320}$Ala mutant (PDB code 1KRC, Table 1) [42] shows an rms deviation of only 0.1 Å from the wild-type KAU. In the active site, the major differences were found to consist in the loss of W170 and a shift of W1 (B-factor = 14 Å^2) from the Ni(2) ion to a Ni-bridging position (Fig. 6). Thus, the coordination geometry of Ni(1) is pseudotetrahedral, while Ni(2) becomes distorted square pyramidal with W1 as the apical ligand. This structure was related to the much lower catalytic activity of the mutant, in addition to the loss of His$^{\alpha 320}$ proposed here to act as the catalytic base, by involving a possible role of His$^{\alpha 320}$ in keeping W1 (through W170) from bridging the two Ni ions, a move that, according to the authors, could hamper urea binding to Ni(1) [42].

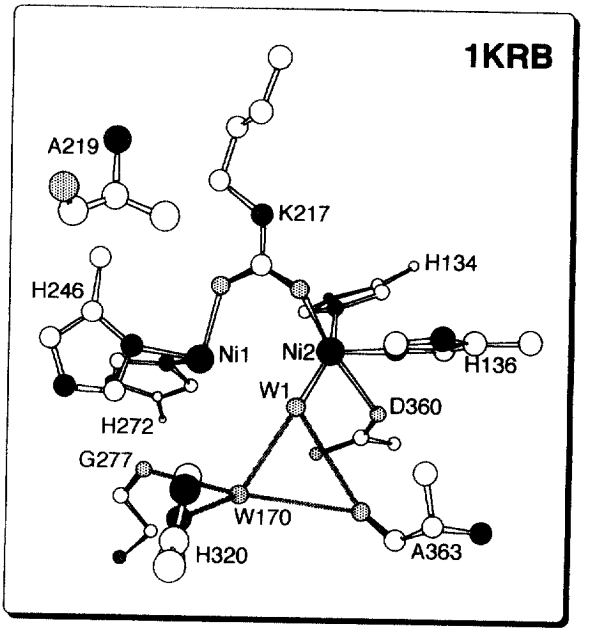

Fig. 5. Model of the active site of KAU His$^{\alpha 219}$Ala mutant, showing the position of selected relevant residues. Atoms and bonds as in Fig. 1. All residues are sized according to their different depths. The PDB code is indicated.

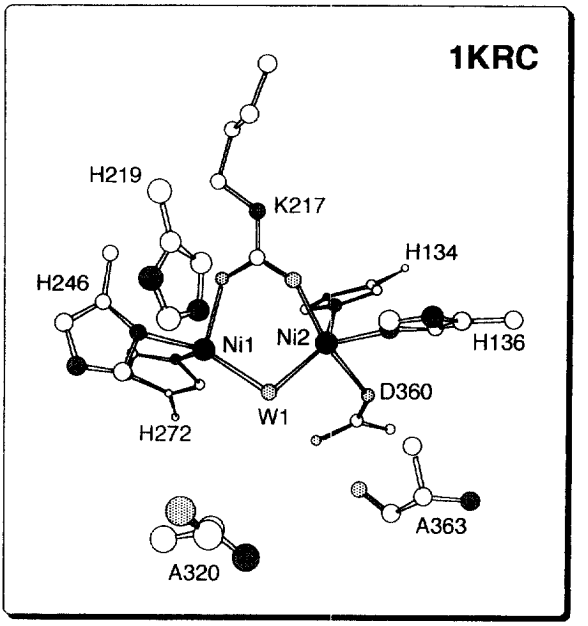

Fig. 6. Model of the active site of KAU $His^{\alpha 320}Ala$ mutant, showing the position of selected relevant residues. Atoms and bonds as in Fig. 1. All residues are sized according to their different depths. The PDB code is indicated.

The removal of one histidine ligand to Ni(2) in the catalytically inactive mutant $His^{\alpha 134}Ala$ [61] resulted in an enzyme lacking Ni(2) and featuring only Ni(1) in the active site (PDB code 1FWI, Table 1) [58]. The $Lys^{\alpha 217*}$ was still carbamylated, and the position of all active site residues (except for the missing $His^{\alpha 134}$) revealed again the substantial rigidity of the structure. The Ni(1) ion has an octahedral geometry, bound to the same ligands as in wild-type urease in addition to three water molecules (Fig. 7). W176 and W177 are well ordered (B-factor = 15 $Å^2$) while W179 is quite disordered (B-factor = 37 $Å^2$). The flexible active site flap was not detected in the electron density, indicating very high thermal disorder.

$Cys^{\alpha 319}$ is located on the flexible flap covering the active site of KAU. This residue is largely conserved in all ureases except for the enzyme from *Staphylococcus xylosus*, which has a threonine in this position [71]. Chemical modification of $Cys^{\alpha 319}$ blocks enzyme activity [72,73], indicating that this residue is somehow involved in catalysis. However, the $Cys^{\alpha 319}Ala$ mutant is still ca. 50% as active as the wild-type urease [74] and structures were determined at pH 6.5 (PDB code 1FWB), pH 7.5 (PDB code 1FWA), pH 8.5 (PDB code 1FWC) and pH 9.4 (PDB code 1FWD) (see Table 1) [63]. There were no significant differences among all these structures. Data obtained at pH 7.5 were refined both including three metal-bound water molecules (one bridging, the other two bound end-on to Ni(1) and Ni(2)) (Fig. 8(A)) and including a metal-bound carbonate (Fig. 8(B)). In the latter case, even though the electron density would account for such a model, the bond angles for the resulting carbonate–metal interactions were very unfavorable [63]. The most evident differences between the structure of $Cys^{\alpha 319}Ala$ mutant and

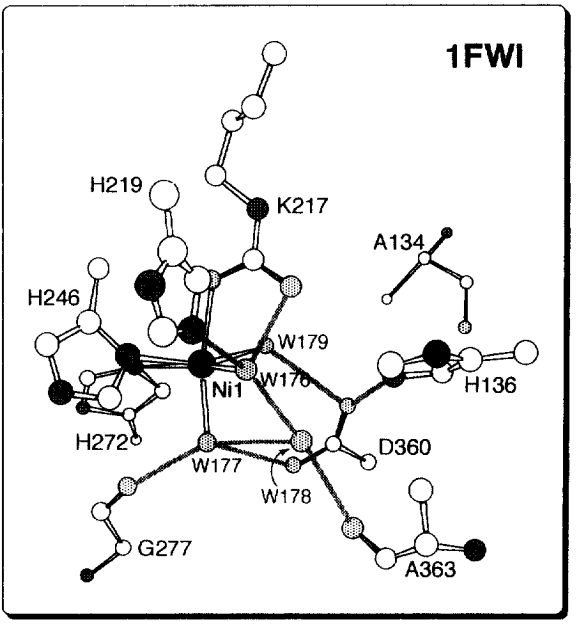

Fig. 7. Model of the active site of KAU His$^{\alpha 134}$Ala mutant, showing the position of selected relevant residues. Atoms and bonds as in Fig. 1. All residues are sized according to their different depths. The PDB code is indicated.

that of the wild-type enzyme involve a much reduced mobility of the flexible flap covering the active site, still found in a 'closed' conformation, but displaying significantly reduced B-factors (from an average value of 38–23 Å^2). In contrast, the structures of Cys$^{\alpha 319}$Asp (PDB code 1FWF), Cys$^{\alpha 319}$Ser (PDB code 1FWG), and Cys$^{\alpha 319}$Tyr (PDB code 1FWH) (see Table 1) displaying respectively, 0.03, 4.5

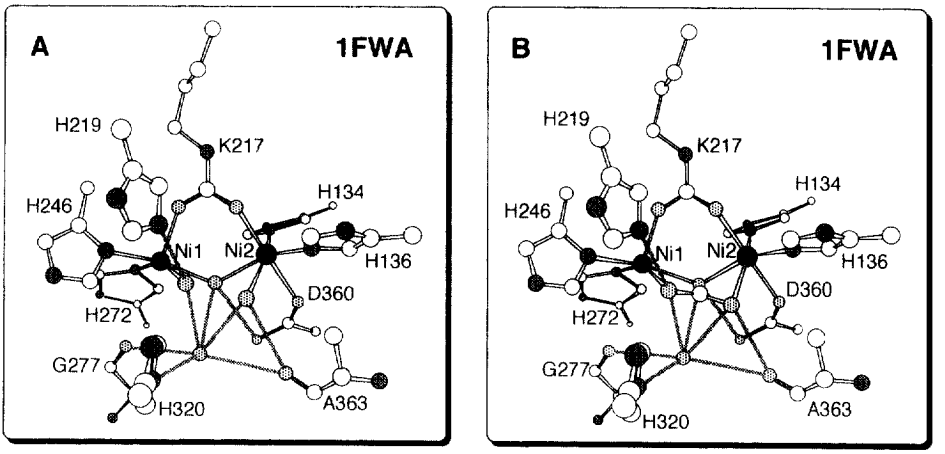

Fig. 8. Model of the active site of KAU Cys$^{\alpha 319}$Ala mutant, showing the position of selected relevant residues. Atoms and bonds as in Fig. 1. All residues are sized according to their different depths. The PDB code is indicated. Panel A: model with three water molecules: Panel B: model with carbonate.

and 0% of the activity observed for the wild-type, indicate a much higher mobility of the flap but the same active site environment [63]. In the case of Cys$^{\alpha 319}$Tyr, the flap is in the same open conformation as for native BPU, an observation that was related to the presence of the bulky tyrosine side chain [63].

To establish the importance of the carbamylated lysine for urease activity, the Lys$^{\alpha 217}$Glu, Lys$^{\alpha 217}$Ala, and Lys$^{\alpha 217}$Cys/Cys$^{\alpha 319}$Ala mutants of KAU were structurally characterized [67]. The structure of Lys$^{\alpha 217}$Glu KAU mutant PDB code 1A5K, Table 1) reveals the complete absence of bound Ni ions, with the Glu side chain being too short to reach the positions designed for the Ni ions in the wild-type enzyme. In place of the metal ions, there are three water molecules in the active site (Fig. 9), while the positions of all other active site residues are unchanged. Analogous features are found in the structure of Lys$^{\alpha 217}$Cys/Cys$^{\alpha 319}$Ala (PDB code 1A5L, Table 1) and Lys$^{\alpha 217}$Ala (PDB code 1A5M, Table 1). All three mutants could be 'chemically rescued' by adding small organic acids and Ni ions: the structures of the Lys$^{\alpha 217}$Ala–formate–Ni complex (PDB code 1A5N, Table 1) (Fig. 10(A)) and Lys$^{\alpha 217}$Cys–formate–Ni complex (PDB code 1A5O, Table 1) (Fig. 10(B)) reveal the presence of a dinuclear Ni center bridged by formate instead of the carbamate group of Lys$^{\alpha 217}$ as in wild-type KAU [67]. In the case of chemically rescued Lys$^{\alpha 217}$Ala mutant, only one ordered water molecule, W502, is detected, and the flexible active site flap is too disordered to be modelled. In the case of chemically rescued Lys$^{\alpha 217}$Ala mutant, the flap is claimed by the authors to be too disordered to be observed in the electron density [67], but it was instead included in the model (PDB code 1A5O).

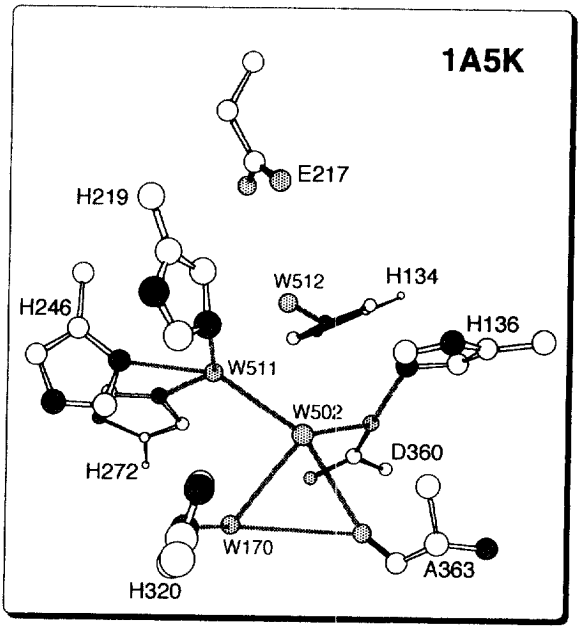

Fig. 9. Model of the active site of KAU Lys$^{\alpha 217}$Glu mutant, showing the position of selected relevant residues. Atoms and bonds as in Fig. 1. All residues are sized according to their different depths. The PDB code is indicated.

5. Crystallographic studies of urease–inhibitor complexes

Cryogenic synchrotron X-ray data collection on a single crystal of BPU inhibited with β-ME has been reported [64], while the structure and binding mode of this

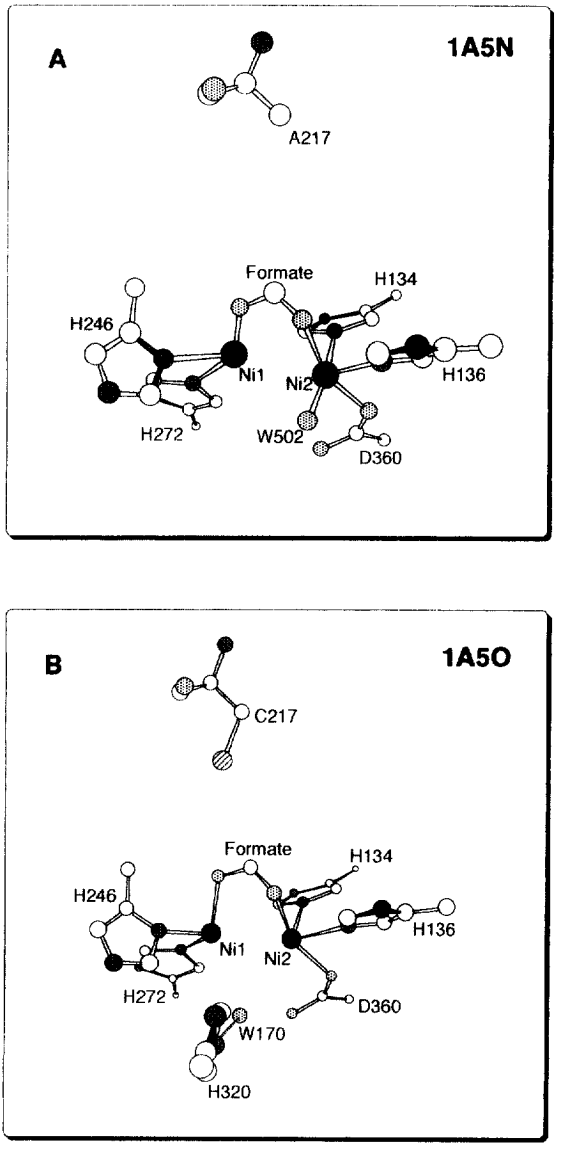

Fig. 10. Model of the active site of KAU Lys$^{\alpha 217}$Ala (A) and Lys$^{\alpha 217}$Cys (B) mutants chemically rescued with formate, showing the position of selected relevant residues. Atoms and bonds as in Fig. 1. All residues are sized according to their different depths. The PDB code is indicated.

inhibitor to the active site (PDB code 1UBP, Table 1) has been recently described [75]. The presence of a bridging atom between the two Ni ions, identified as the sulfur of β-ME, is evident in the electron density. The refined model of the inhibitor indicates a chelate binding mode through the terminal OH group, coordinated to Ni(1) (Fig. 11). Both Ni ions in β-ME-inhibited BPU appear to be pentacoordinated. The coordination geometry around Ni(1) is distorted square-pyramidal, with the equatorial plane constituted by the S and O atoms of β-Me, by the Oθ1 atom of the bridging carbamylated $Lys^{\alpha 220*}$, and by the Nε of $His^{\alpha 275}$, the apical ligand being the Nδ of $His^{\alpha 249}$. In contrast, the coordination geometry of Ni(2) is best described as distorted trigonal bipyramidal, with the equatorial plane constituted by the bridging S atom of β-ME and by the Nε atoms of $His^{\alpha 137}$ and $His^{\alpha 139}$, the opposite apical ligands being the Oθ2 atom of the bridging carbamylated lysine and $Asp^{\alpha 363}$ Oδ1. The equatorial planes of the square and trigonal pyramids are joined through the bridging S atom of β-ME, with a dihedral angle between the two average equatorial planes of 63°. The coordination distances between the Ni ions and their protein ligands are, within experimental error, the same as those obtained from the X-ray structure [65] and from EXAFS data on native BPU [53]. This

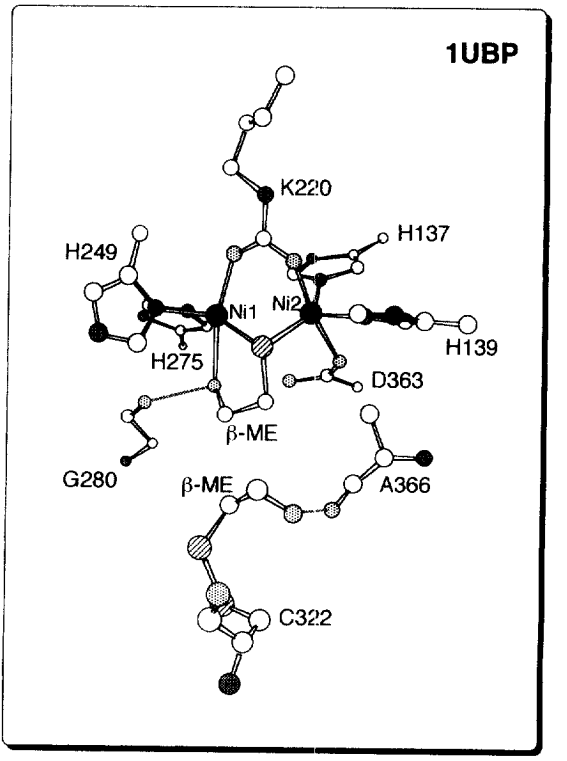

Fig. 11. Model of the active site of BPU inhibited with β-ME, showing the position of selected relevant residues. Atoms and bonds as in Fig. 1. All residues are sized according to their different depths. The PDB code is indicated.

observation suggests substantial rigidity of the Ni coordination spheres in this enzyme.

Charge-transfer transitions observed in the near-UV [44], CD [76], and MCD [62] spectra of urease in the presence of thiolate competitive inhibitors have been interpreted in the past as indicating direct binding to the Ni(II) ions. Magnetic susceptibility and variable temperature MCD spectra of β-ME-inhibited urease had shown that the Ni centres are strongly antiferromagnetically exchange-coupled [48,62], suggesting the presence of a thiolate bridging ligand. This observation was further supported by EXAFS [47,50]. The structure of β-ME-inhibited BPU is in agreement with the spectroscopic results, directly revealing the presence of a thiolate ligand bridging the two Ni ions. The determination of the crystal structure of β-ME-inhibited BPU further shows the unexpected chelating coordination mode of β-ME to the Ni ions. The torsional angle of the β-ME molecule is 59°. The ROH–Ni(1) interaction is assisted and stabilized by a strong hydrogen bond donated to the carbonyl oxygen of the conserved $Gly^{\alpha 280}$ (at 2.4 Å). β-ME is a poor chelating agent due to the low Lewis base character of its OH group, but the hydrogen bond with $Gly^{\alpha 280}$ enhances the basicity of the hydroxyl oxygen and facilitates binding to Ni(1).

Fig. 11 shows that, in β-ME-inhibited BPU, a second molecule of β-ME is involved in a mixed disulfide bond with $Cys^{\alpha 322}$, a residue which is supposed to play a significant role in the catalytic process [72,73], even though it is not essential [74,77]. $Cys^{\alpha 322}$ resides on the mobile flap, closed in native KAU and open in native BPU. In β-ME-inhibited BPU, the flap is open [75]. This flap has been proposed to act as a gate for the entrance of the substrate to the active site [59,63] but could also take part in the assembly of the dinickel centre from apo-urease, for example through the conserved $Cys^{\alpha 322}$, acting, in this case, as a Ni shuttle. The β-ME molecule forming the mixed disulfide with $Cys^{\alpha 322}$ in β-ME-inhibited BPU is further involved in a hydrogen bond between its α-hydroxyl group and the carbonyl oxygen atom of $Ala^{\alpha 366}$, positioned on a neighboring loop (Fig. 11). This interaction reduces the flexibility of the flap, and the resulting network seals the entrance to the active site by steric hindrance. In summary, the X-ray structure of β-ME-inhibited BPU reveals that inhibition occurs by targeting enzyme sites that both directly (the metal centres) and indirectly (the cysteine side chain) participate in substrate positioning and activation. This double inhibition mode is likely to be involved in all examples in which a thiol acts as urease inhibitor [72,78].

The structure of a KAU mutant urease ($Cys^{\alpha 319}Ala$) complexed with the competitive inhibitor acetohydroxamic acid (AHA) (PDB code 1FWE, Table 1) has been reported [63]. In this model, the protein ligands to the Ni ions are invariant as compared with the native form. In analogy with the structure of β-ME-inhibited BPU, the negatively charged hydroxamate oxygen bridges the two Ni ions, while the carbonyl oxygen of AHA is further bound to Ni(1) at 2.0 Å, in a chelate mode (Fig. 12). The Ni–Ni distance is 3.7 Å, suggesting that this separation does not vary substantially upon inhibitor binding. The active site flap is highly disordered, and its electron density was not modeled. A pronounced asymmetry was reported for

the Ni-bridging atom (Ni(1)–O = 2.6 Å; Ni(2)–O = 1.8 Å). The coordination mode of AHA to the active site of KAU is analogous to the structure of a synthetic model compound [79], which however, shows the presence of a molecule of AHA symmetrically bridging the two Ni ions. Preliminary results on AHA-inhibited BPU (at 1.55 Å resolution) reveal the presence of a symmetric bridge [80], which is consistent with the synthetic model.

6. Crystallographic study of a transition state analogue bound to urease

A good transition state analogue for the enzymatic hydrolysis of urea is the tetrahedral diamidophosphate $(NH_2)_2PO_2^-$ (DAP). Evidence that, in the presence of PPD $(NH_2)_2PO(OPh)$ (PPD), the actual inhibitor of urease is DAP, produced by the enzymatic hydrolysis of PPD to yield phenol, was previously suggested by kinetic experiments [81]. The latter also indicated that the urease–DAP complex formed during the enzymatic hydrolysis of PPD is much tighter than the urease–DAP complex formed by simply adding DAP to urease, suggesting the presence of two isomeric complexes. The lability of the non-enzymatically derived urease–DAP complex may prevent its formation and crystallization. Therefore, BPU was crystallized in the presence of PPD, and the structure thus obtained has been recently reported (PDB code 3UBP, Table 1) [65]. This structure reveals that in the active site the positions of all Ni-bound protein residues do not significantly differ from

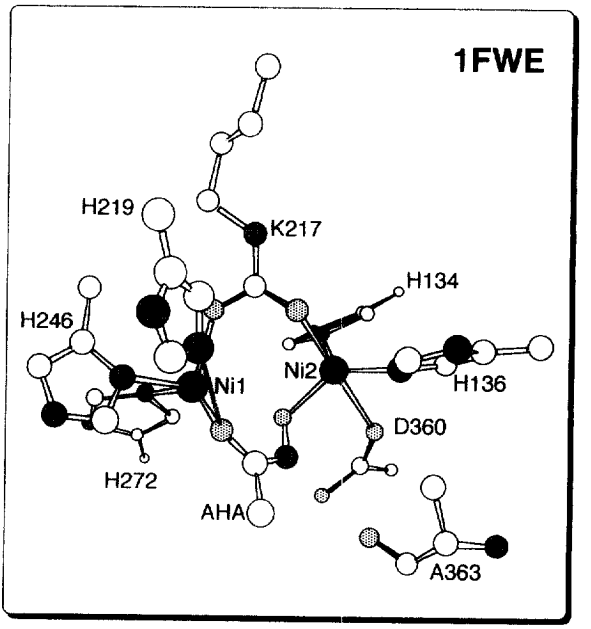

Fig. 12. Model of the active site of KAU $Cys^{\alpha 319}Ala$ mutant inhibited with AHA, showing the position of selected relevant residues. Atoms and bonds as in Fig. 1. All residues are sized according to their different depths. The PDB code is indicated.

the structure of native BPU. The residual electron density maps show the presence of a tetrahedrally shaped molecule bound to the dinickel center through three atoms: one symmetrically bridges the two Ni ions, while each of the other two bind one Ni. The tetrahedral molecule has replaced the cluster of four water/hydroxide molecules found in native BPU. Clearly, the bound inhibitor is not the PPD molecule, due to the absence of electron density accounting for an aromatic ring. The absence of sulfate or phosphate in the crystallization buffer ruled out the possibility that these anions could account for the tetrahedral electron density observed. In addition, the presence of sulfate was ruled out by the scarce electron density in the center of the tetrahedron, not accounting for the heavy sulfur atom. Therefore, the electron density found in the structure of inhibited urease was modeled with DAP (Fig. 13). In DAP-inhibited BPU, the flap is in the closed conformation, essentially identical to that found in native KAU. A remarkably specific hydrogen bonding pattern stabilizes the inhibitor and directs its orientation in the cavity, allowing the unambiguous assignment of all DAP atoms to either oxygen or nitrogen. DAP is bound to Ni(1) and to Ni(2) through one oxygen and one nitrogen atom, respectively. The second DAP oxygen atom symmetrically bridges the two nickels, while the second nitrogen atom points away towards the cavity opening. The Ni(1)-bound oxygen atom receives an hydrogen bond from $His^{\alpha 222}$ Nε (at 2.6 Å), whose protonation state is determined in analogy with the structure of native BPU. In contrast, the Ni(2)-bound DAP amido nitrogen forms

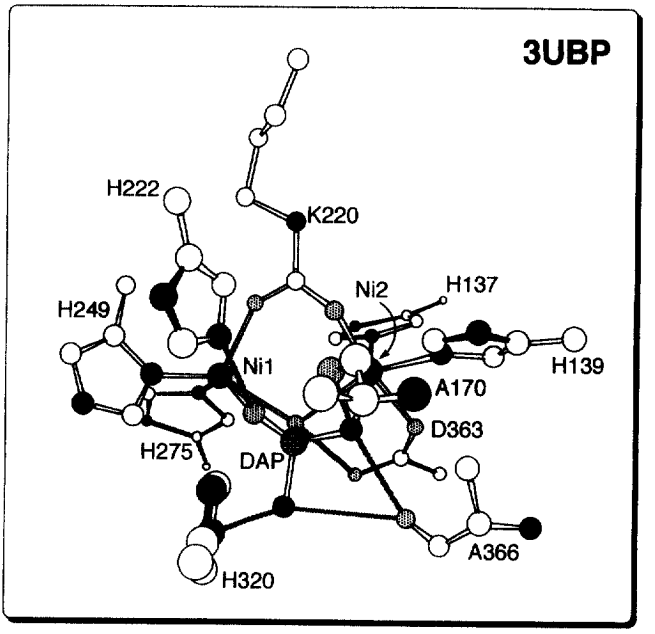

Fig. 13. Model of the active site of BPU inhibited with DAP, showing the position of selected relevant residues. Atoms and bonds as in Fig. 1. All residues are sized according to their different depths. The PDB code is indicated.

two hydrogen bonds, donated to the carbonyl oxygen atoms of Ala$^{\alpha 170}$ (at 2.9 Å) and Ala$^{\alpha 366}$ (at 2.8 Å). Furthermore, the distal DAP nitrogen donates a bifurcated hydrogen bond to Ala$^{\alpha 366}$ and Gly$^{\alpha 280}$ carbonyl oxygens, both at 3.1 Å, and to His$^{\alpha 323}$ Nε (3.3 Å). Finally, the Ni-bridging DAP oxygen atom is at hydrogen bonding distance from the Asp$^{\alpha 363}$ Oδ2 atom (2.4 Å). The assignment of the shared proton to either DAP or to Asp$^{\alpha 363}$ Oδ2 is not easy to determine by considering the similar pK_a values for aspartate and DAP (4.83 [82]).

7. A novel proposal for the urease mechanism

The most widely accepted mechanism of urease is based on different roles played by the two Ni(II) ions: one of them binding and activating urea, the other binding and activating the nucleophile water [2,57,59,83]. In particular, in view of the crystal structure of native KAU and of its mutants, it was proposed that urea binds to the five-coordinate Ni(1) while the hydroxide ion, bound to the hexa-coordinate Ni(2), acts as nucleophile [57,59]. This model entails a reaction intermediate which would bridge the two Ni ions in a bidentate mode through two O atoms (Fig. 14(A)). However, it has been recognized that this mechanism raises two problems [59]: one about the missing general base with pK_a 9.0 [13,51,68,83] which would deprotonate the Ni(2)-bound water molecule (pK_a 10.6) at the optimum pH for enzyme activity (pH 8), and the second about the role of His$^{\alpha 323}$ as general acid, which must be protonated at pH 8 even though it has a pK_a of 6.5 [61]. These

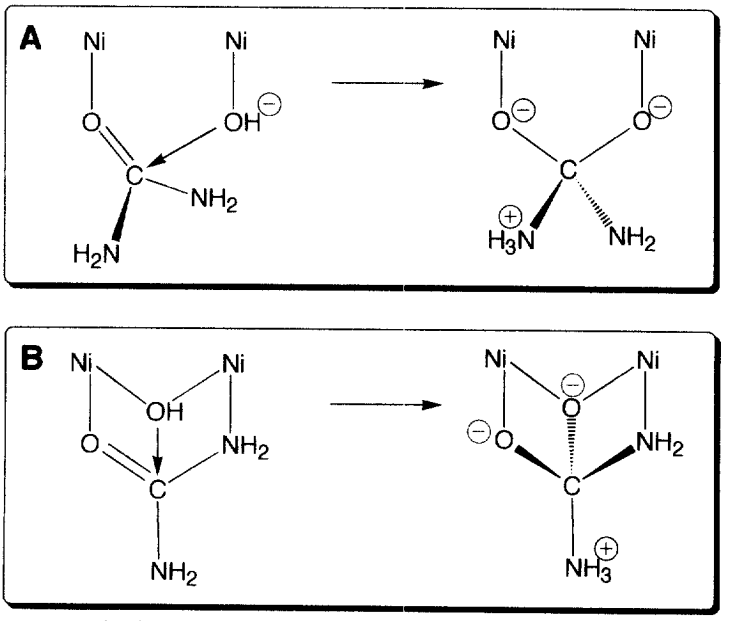

Fig. 14. The urease mechanism as proposed by Karplus and Hausinger (A) and by the present authors (B) showing the model of the transition state structures obtained in the two cases. The contrast between the transition state proposed for mechanism A and the X-ray structure of DAP-inhibited BPU, and the analogy of the latter with the transition state obtained following model B, is evident.

inconsistencies forced the introduction of the 'reverse protonation hypothesis' [59], which, however, would result in only 0.3% of all urease molecules being in the optimal protonation state for catalysis.

The crystal structures of native and DAP-inhibited BPU urease provide information on the enzyme in the resting state and in a complex with a transition state analogue useful to deduce a novel mechanism for urease [65]. The presence of the tetrahedral water/hydroxide cluster in the proximity of the dinickel center in the native enzyme, together with the binding mode of DAP, suggest an accurate design of the enzyme active site to bind the substrate in an orientation-specific mode, and subsequently to stabilize a tetrahedral transition state. According to this proposal, urea enters the active site cavity in the 'open' conformation of the flap, replacing W1, W2, and W3, located in positions matching its molecular shape and dimensions (Fig. 15(A,B)). The hydrogen bonding network that stabilizes the binding of DAP to the active site orientates the substrate in the catalytic cavity. Urea binds the more electrophilic five-coordinated Ni(1) with the carbonyl oxygen, approaching the six-coordinated Ni(2) with one of its amino groups. The protonation state of

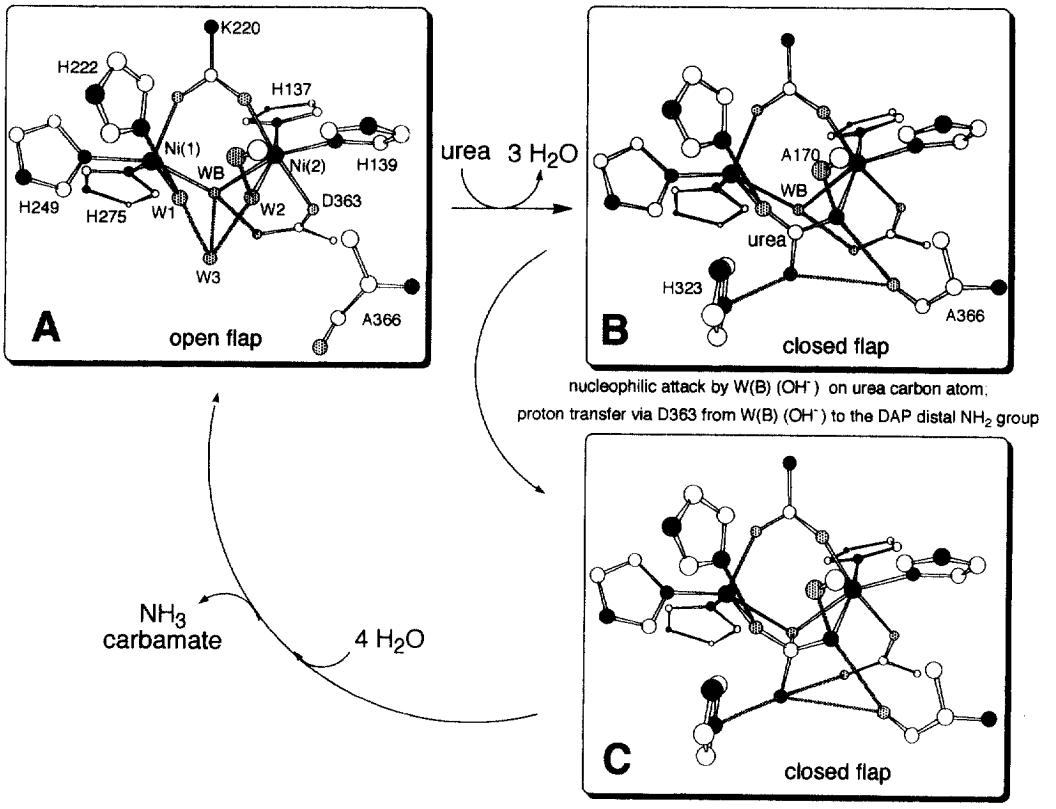

Fig. 15. The new proposed mechanism for urease. Only the essential atoms of the Ni ligands and of relevant amino acids involved in the mechanism are shown. (A) Model of the resting enzyme taken from the crystal structure of native BPU. (B) Proposed urea binding mode obtained by modeling the substrate into the cavity of the DAP-inhibited BPU. (C) Model for the transition state of urea hydrolysis built from the crystal structure of DAP-inhibited BPU.

$His^{\alpha 222}$ Nε stabilizes the binding of urea carbonyl O atom to Ni(1). The change from the 'open' to the 'closed' conformation of the flexible flap induces a rearrangement of $Ala^{\alpha 366}$ carbonyl group such that its oxygen atom points towards Ni(2) (Fig. 15(B)). As a consequence, the carbonyl groups of $Ala^{\alpha 170}$ and $Ala^{\alpha 366}$ are positioned to act as hydrogen bond acceptors towards the urea NH_2 group, thereby assisting its binding to Ni(2) in a way similar to that observed for β-ME. Urea is a poor chelating ligand because of the low Lewis base character of its NH_2 groups; however, the hydrogen bonds with the nearby carbonyl oxygens enhances the basicity of the amino group and facilitate its binding to Ni(2). In conclusion, according to this mechanism, the position and orientation of the substrate are induced both by the asymmetric structural features of the active site residues, positioned in order to act as hydrogen bond donors in the vicinity of Ni(1) and as hydrogen bond acceptors in the vicinity of Ni(2), and by the conformational change of the flap.

The bidentate ligation of urea to the two very electrophilic Ni(II) ions, together with the hydrogen bonding network described, strongly activates the inert urea molecule towards nucleophilic attack, by polarizing the C–O and the C–NH_2 bonds. This binding mode of the substrate brings the urea carbon in close proximity to the Ni-bridging ligand, proposed here to be the nucleophile in the form of a hydroxide anion, further activated by its hydrogen bond to $Asp^{\alpha 363}$ Oδ2 (Fig. 15(B,C)). Here, the mechanism can also be described as an electrophilic attack of the activated urea carbon onto the Ni-bridging hydroxide (Fig. 14(B)). In the 'closed' conformation of the flap, $His^{\alpha 323}$ is in the proper position to interact with the transition state/product of the reaction as shown in Fig. 15(C). The proposed tetrahedral transition state, generated upon bond formation between the bridging hydroxide and the urea carbon, is mimicked by DAP. In this process, $His^{\alpha 222}$ and $His^{\alpha 323}$ act by stabilizing, respectively, the negative and positive charges developing on the tetrahedral intermediate. The proton needed by the distal urea NH_2 group in order to induce cleavage of the C–N bond and release of ammonia, can easily be provided by the hydroxide nucleophile itself, whose pK_a is decreased by the formation of the C–O bond, in a proton transfer assisted by $Asp^{\alpha 363}$ Oδ2, which could be now hydrogen bonded to the nascent ammonia (Fig. 15(B,C)). In the final step, ammonia is released from the active site, possibly assisted by the movement of $His^{\alpha 323}$ when the flexible flap opens. The resulting negatively charged carbamate is then released because of its unfavorable interaction with $Asp^{\alpha 363}$ Oδ2, in a process assisted by the movement of the positively charged $Arg^{\alpha 339}$ upon flap opening.

This novel mechanism [65] overcomes the problems encountered by the mechanism proposed by Karplus and Hausinger [59]: the bridging hydroxide is considered to be both the nucleophile and the general acid, while $His^{\alpha 323}$ acts as a general base, not by deprotonating the hydrolytic water, but by stabilizing the positive charge which develops on the transition state. This model is consistent both with a role in substrate binding for $His^{\alpha 222}$ [61] and with the pH dependence of k_{cat}, featuring apparent pK_a values near 6.5 and 9 [13,51,68,83]. The latter pK_a, still not assigned to any active site residues, is attributed to the deprotonation of the bridging hydroxide anion, whose hydrogen is needed, according to our model, to protonate the distal amido group and yield ammonia. Furthermore, the proposed transition state bind-

ing mode is consistent with a binding energy larger than 19 kcal mol^{-1} as demanded by the enzyme proficiency greater than 10^{14} [59], because the proposed binding of the transition state involves three coordination bonds to the Ni ions and at least five hydrogen bonding interactions. The structure of DAP-inhibited BPU suggests a binding mode for the transition state analogue that is not consistent with the mechanism proposed by Karplus and Hausinger, due to the presence of an oxygen atom of DAP that bridges the two Ni ions, excluding the possibility that the two substrates, urea and water, initially reside on two different Ni ions (Fig. 14). Finally, recent docking studies have produced structures for urea bound to the 'open' and 'closed' conformation of the flap that are fully consistent with this proposal [84].

This model provides a rationale for the presence of a bimetallic active site in urease, as well as explaining the requirement for Ni^{2+} ions, in place of the more common Zn^{2+} in hydrolytic enzymes. Ni^{2+} ions are characterized by higher affinity toward nitrogenous-based ligands than Zn^{2+} [85], thereby stabilizing the binding of a urea NH_2 group. In addition, the presence of a bimetallic center, with the Ni^{2+} ions possessing multiple available binding sites due to their preference for octahedral coordination sphere (as opposed to Zn^{2+}, mostly tetrahedral), would represent a requirement for both the bridging-binding mode of urea and for stabilization of the metal ion binding to the protein through multiple sites for amino acids ligands.

The overall architecture of urease reveals striking similarities to other enzymes such as adenosine deaminase, dihydroorotases, allantoinases, hydantoinases, AMP deaminase, adenine deaminase, cytosine deaminase, imidazolonepropionase, aryldialkyl–phosphatases, chlorohydrolase, formylmethanefuran dehydrogenases, and proteins involved in animal neuronal development [86]. The proposed novel mechanistic model, whose main feature is the role of the metal-bridging hydroxide acting as the nucleophile, may well constitute a general rule for all hydrolytic enzymes containing similar catalytic sites [87], and therefore could potentially lead to precise predictions for the mechanism of action of a broad ensemble of evolutionarily distant enzymes.

References

[1] H.A. Krebs, K. Henseleit, Hoppe-Seyler's Z. Physiol. Chem. 210 (1932) 33.
[2] B. Zerner, Bioorg. Chem. 19 (1991) 116.
[3] J.B. Sumner, J. Biol. Chem. 69 (1926) 435.
[4] N.E. Dixon, C. Gazzola, R. Blakeley, B. Zerner, J. Am. Chem. Soc. 97 (1975) 4131.
[5] H.L. Drake, S.-I. Hu, H.G. Wood, J. Biol. Chem. 255 (1980) 7174.
[6] G. Diekert, B. Klee, R.K. Thauer, Arch. Microbiol. 124 (1980) 103.
[7] W.B. Whitman, R.S. Wolfe, Biochem. Biophys. Res. Commun. 92 (1980) 1196.
[8] J.R. Lancaster Jr., Science 216 (1982) 1324.
[9] D. Qiu, M. Kumar, S.W. Ragsdale, T.G. Spiro, J. Am. Chem. Soc. 118 (1996) 10429.
[10] H.-D. Youn, E.-J. Kim, J.-H. Roe, Y.C. Hah, S.-O. Kang, Biochem. J. 318 (1996) 889.
[11] H.-D. Youn, H. Youn, J.-W. Lee, Y.-I. Yim, J.-K. Lee, Y.C. Hah, S.-O. Kang, Arch. Biochem. Biophys. 334 (1996) 341.

[12] R.P. Hausinger, Microbiol. Rev. 51 (1987) 22.
[13] H.L.T. Mobley, R.P. Hausinger, Microbiol. Rev. 53 (1989) 85.
[14] R.P. Hausinger, Biochemistry of Nickel, Plenum, New York, 1993, pp. 23–57.
[15] R.K. Andrews, R.L. Blakeley, B. Zerner, in: J.R. Lancaster Jr. (Ed.), The Bioinorganic chemistry of Nickel, VCH, New York, pp. 141–146.
[16] H.L.T. Mobley, M.D. Island, R.P. Hausinger, Microbiol. Rev. 59 (1995) 451.
[17] C.M. Collins, S.E.F. D'Orazio, Mol. Microbiol. 9 (1993) 907.
[18] P.J. Stangel, in: R.D. Hauck (Ed.), Nitrogen in Crop Production, American Society of Agronomy, Madison, WI, 1984, pp. 23–54.
[19] A.B. Lloyd, J.M. Sheaffe, Plant Soil 39 (1973) 71.
[20] M.I. Zantua, J.M. Bremner, Soil. Biol. Biochem. 9 (1977) 135.
[21] J.M. Bremner, R.L. Mulvaney, in: R.G. Burns (Ed.), Soil Enzymes, Academic Press, New York, 1978, pp. 149–196.
[22] R.G. Burns, in: P.M.a.S.M. Huang (Ed.), Interactions of Soil Minerals with Natural Organics and Microbes, vol. special publication n.17, Soil Science Society of America, Madison, WI, 1986, pp. 429–452.
[23] I.J.M. Rosenstein, J.M.T. Hamilton-Miller, Crit. Rev. Microbiol. 11 (1984) 1.
[24] K.L. Sahrawat, Plant Soil 57 (1980) 335.
[25] R.L. Mulvaney, J.M. Bremner, in: E.A. Paul, J.N. Ladd (Eds.), Soil Biochemistry, vol. 5, Marcel Dekker, New York, 1981, pp. 153–196.
[26] R.D. Hauck, in: R.D. Hauck (Ed.), Nitrogen in Crop Production, American Society of Agronomy, Madison, WI, 1984, pp. 551–560.
[27] D.A. Martens, J.M. Bremner, Soil. Sci. Soc. Am. J. 48 (1984) 302.
[28] R.D. Voss, in: R.D. Hauck (Ed.), Nitrogen in Crop Production, American Society of Agronomy, Madison, WI, 1984, p. 571.
[29] J.M. Bremner, M.J. Krogmeier, Proc. Nat. Acad. Sci. USA 85 (1988) 4601.
[30] G.W. McCarthy, J.M. Bremner, J.S. Lee, Plant Soil 127 (1990) 269.
[31] J.M. Bremner, Fert. Res. 42 (1995) 321.
[32] J.M. Bremner, H.S. Chai, Commun. Soil Sci. Anal 17 (1986) 337.
[33] G.W. McCarthy, J.M. Bremner, H.S. Chai, Biol. Fert. Soils 8 (1989) 123.
[34] J.M. Bremner, H.S. Chai, Biol. Fert. Soils 8 (1989) 227.
[35] K.F. Bronson, J.T. Touchton, A.E. Hiltbold, L.L. Hendrickson, Comm. Soil Sci. Plant Anal. 20 (1989) 1439.
[36] K.F. Bronson, J.T. Touchton, C.G. Cummings, L.L. Hendrickson, J. Fert. Issues 7 (1990) 31.
[37] L.L. Hendrickson, E.A. Douglass, Soil. Biol. Biochem. 25 (1993) 1613.
[38] D.P. Griffith, Kidney Int. 13 (1978) 372.
[39] E. Sim, A. Jones, L. Stanley, Acta Pharmacol. Toxicol. 57 (1985) 304.
[40] M.J. Krogmeier, G.W. McCarty, J.M. Bremner, Proc. Natl. Acad. Sci. USA 86 (1989) 1110.
[41] J.M.T. Hamilton-Miller, R.A. Gargan, Invest. Urol. 16 (1979) 327.
[42] E. Jabri, P.A. Karplus, Biochemistry 35 (1996) 10616.
[43] N.E. Dixon, R.L. Blakeley, B. Zerner, Can. J. Biochem. 58 (1980) 481.
[44] R.L. Blakeley, N.E. Dixon, B. Zerner, Biochim. Biophys. Acta 744 (1983) 219.
[45] S.S. Hasnain, B. Piggot, Biochem. Biophys. Res. Commun. 112 (1983) 279.
[46] L. Alagna, S.S. Hasnain, B. Piggot, D.J. Williams, Biochem. J. 220 (1984) 591.
[47] P.A. Clark, D.E. Wilcox, R.A. Scott, Inorg. Chem. 29 (1990) 579.
[48] P.A. Clark, D.E. Wilcox, Inorg. Chem. 28 (1989) 1326.
[49] E.P. Day, J. Peterson, M.S. Sendova, M.J. Todd, R.P. Hausinger, Inorg. Chem. 32 (1993) 634.
[50] S. Wang, M.H. Lee, R.P. Hausinger, P.A. Clark, D.E. Wilcox, R.A. Scott, Inorg. Chem. 33 (1994) 1589.
[51] M.J. Todd, R.P. Hausinger, J. Biol. Chem. 262 (1987) 5963.
[52] S. Benini, C. Gessa, S. Ciurli, Soil Biol. Biochem. 28 (1996) 819.
[53] S. Benini, S. Ciurli, H.F. Nolting, S. Mangani, Eur. J. Biochem. 239 (1996) 61.
[54] S.B. Mulrooney, R.P. Hausinger, J. Bacteriol. 172 (1990) 5837.
[55] G. Moersdorf, P. Weinmann, H. Kaltwasser, EMBL Data Library, X78411, 1994.

[56] K. Takishima, T. Suga, G. Mamiya, Eur. J. Biochem. 175 (1988) 151.
[57] E. Jabri, M.B. Carr, R.P. Hausinger, P.A. Karplus, Science 268 (1995) 998.
[58] I.-S. Park, L.O. Michel, M.A. Pearson, E. Jabri, P.A. Karplus, S. Wang, J. Dong, R.A. Scott, B.P. Koehler, M.K. Johnson, R.P. Hausinger, J. Biol. Chem. 271 (1996) 18632.
[59] P.A. Karplus, M.A. Pearson, R.P. Hausinger, Acc. Chem. Res. 30 (1997) 330.
[60] I.-S. Park, R.P. Hausinger, J. Protein Chem. 12 (1993) 51.
[61] I.-S. Park, R.P. Hausinger, Protein Sci. 2 (1993) 1034.
[62] M.G. Finnegan, A.T. Kowal, M.T. Werth, P.A. Clark, D.E. Wilcox, M.K. Johnson, J. Am. Chem. Soc. 113 (1991) 4030.
[63] M.A. Pearson, L. Overbye Michel, R.P. Hausinger, P.A. Karplus, Biochemistry 36 (1997) 8164.
[64] S. Benini, S. Ciurli, W. Rypniewski, K.S. Wilson, S. Mangani, Acta Crystallogr. D54 (1998) 409.
[65] S. Benini, W.R. Rypniewski, K.S. Wilson, S. Miletti, S. Ciurli, S. Mangani, Structure 7 (1999) 205.
[66] M.B.C. Moncrief, L.G. Hom, E. Jabri, P.A. Karplus, R.P. Hausinger, Protein Sci. 4 (1995) 2234.
[67] M.A. Pearson, R.A. Schaller, L.O. Michel, P.A. Karplus, R.P. Hausinger, Biochemistry 37 (1998) 6214.
[68] S. Ciurli, C. Marzadori, S. Benini, S. Deiana, C. Gessa, Soil Biol. Biochem. 28 (1996) 811.
[69] F. Basolo, R.G. Pearson, Mechanisms of Inorganic Reactions, Wiley, New York, 1967, pp. 31–33.
[70] F.H. Allen, O. Kennard, Chem. Des. Automation News 8 (1993) 31.
[71] J. Jose, S. Christians, R. Rosenstein, F. Gotz, H. Kaltwasser, FEMS Microbiol. Lett. 80 (1991) 277.
[72] M.J. Todd, R.P. Hausinger, J. Biol. Chem. 266 (1991) 10260.
[73] M.J. Todd, R.P. Hausinger, J. Biol. Chem. 266 (1991) 24327.
[74] P.R. Martin, R.P. Hausinger, J. Biol. Chem. 267 (1992) 20024.
[75] S. Benini, W.R. Rypniewski, K.S. Wilson, S. Ciurli, S. Mangani, J. Biol. Inorg. Chem. 3 (1998) 268.
[76] K. Nagarajam, W.N. Fishbein, Fed. Proc. Fed. Am. Soc. Exp. Biol. 36 (1977) 700.
[77] J. Jose, K. Schafer, H. Kaltwasser, Arch. Microbiol. 161 (1994) 384.
[78] M.J. Todd, R.P. Hausinger, J. Biol. Chem. 264 (1989) 15835.
[79] A.J. Stemmler, J.W. Kampf, M.L. Kirk, V.L. Pecoraro, J. Am. Chem. Soc. 117 (1995) 6368.
[80] S. Benini, W.R. Rypniewski, K.S. Wilson, S. Miletti, S. Ciurli, S. Mangani (1999), in preparation.
[81] R.K. Andrews, A. Dexter, R.L. Blakeley, B. Zerner, J. Am. Chem. Soc. 108 (1986) 7124.
[82] R. Klement, G. Biberacher, V. Hille, Z. Anorg. Chem. 289 (1957) 80.
[83] N.E. Dixon, P.W. Riddles, C. Gazzola, R.L. Blakeley, B. Zerner, Can. J. Biochem. 58 (1980) 1335.
[84] F. Musiani, S. Benini, S. Ciurli (1999), in preparation.
[85] R.M. Smith, A.E. Martell, Critical Stability Constants, vol. 2: Amines, Plenum, New York and London, 1975.
[86] L. Holm, C. Sander, Proteins Struct. Funct. Gen. 28 (1997) 72.
[87] D.E. Wilcox, Chem. Rev. 96 (1996) 2435.